The Potential for an Enhanced Role For MRI in Radiation-therapy Treatment Planning

The exquisite soft-tissue contrast of magnetic resonance imaging (MRI) has meant that the technique is having an increasing role in contouring the gross tumor volume (GTV) and organs at risk (OAR) in radiation therapy treatment planning systems (TPS). MRI-planning scans from diagnostic MRI scanners are currently incorporated into the planning process by being registered to CT data. The soft-tissue data from the MRI provides target outline guidance and the CT provides a solid geometric and electron density map for accurate dose calculation on the TPS computer. There is increasing interest in MRI machine placement in radiotherapy clinics as an adjunct to CT simulators. Most vendors now offer 70 cm bores with flat couch inserts and specialised RF coil designs. We would refer to these devices as MR-simulators. There is also research into the future application of MR-simulators independent of CT and as in-room image-guidance devices. It is within the background of this increased interest in the utility of MRI in radiotherapy treatment planning that this paper is couched. The paper outlines publications that deal with standard MRI sequences used in current clinical practice. It then discusses the potential for using processed functional diffusion maps (fDM) derived from diffusion weighted image sequences in tracking tumor activity and tumor recurrence. Next, this paper reviews publications that describe the use of MRI in patient-management applications that may, in turn, be relevant to radiotherapy treatment planning. The review briefly discusses the concepts behind functional techniques such as dynamic contrast enhanced (DCE), diffusion-weighted (DW) MRI sequences and magnetic resonance spectroscopic imaging (MRSI). Significant applications of MR are discussed in terms of the following treatment sites: brain, head and neck, breast, lung, prostate and cervix. While not yet routine, the use of apparent diffusion coefficient (ADC) map analysis indicates an exciting future application for functional MRI. Although DW-MRI has not yet been routinely used in boost adaptive techniques, it is being assessed in cohort studies for sub-volume boosting in prostate tumors.

Key words: MRI; Radiation therapy; Radiation; Therapy treatment planning.

Abbreviations: ADC: Apparent Diffusion Coefficient; AVM: Arteriovenous Malformation; BOLD: Blood Oxygen Level Dependent; CC: Corpus Carvernosum; CT: Computed Tomography; CTV: Clinical Target Volume; 4DCT: 4 Dimensional Computed Tomography; DW: Diffusion Weighted; DCE: Dynamic Contrast Enhanced; DNP: Dynamic Nuclear Polarization; EPI: Echo Planar Imaging; fDM: Functional Diffusion Map; fV: Functional Lung Volume; FFE-EPI: Fast Field Echo Planar Imaging; FIESTA: Fast Image Employing Steady State Acquisition; FLASH: Fast Low Angle Shot; FLAIR: Fast Fluid-attenuated Inversion Recovery; fMRI: Functional Magnetic Resonance Imaging; FSRT: Fractionated Stereotactic Radiation Therapy; GTV: Gross Tumor Volume; HNSCC: Head and Neck Squamous Cell Carcinioma; IGBT: Image Guided Brachytherapy; IPA: Internal Pudental Artery; MRA: Magnetic Resonance Angiography; MRI: Magnetic Resonance Imaging; MRSI: Magnetic Resonance Spectroscopic Imaging; NSCLC: Non Small Cell Lung Cancer; PET: Positron Emission Tomography; PHIP: Parahydrogen Induced Polarization; PTV: Planning Target Volume; SPGR: Spoiled Gradient; SSFSE: Single Shot Fast Spin Echo; SRS: Stereotactic Radiosurgery; T1: Longitudinal Relaxation Time; T2: Transverse Relaxation Time; TB: Tumor Bed; TPS: Treatment Planning System; TR: Repetition Time; TrueFIST: True Fast Imaging with Steady State Precession; VMAT: Volumetric Modulated Arc Therapy.

P. Metcalfe, Ph.D.[1]*
G. P. Liney, Ph.D.[2,3]
L. Holloway, Ph.D.[1,3,4,5]
A. Walker, B.Sc.(hons)[1]
M. Barton, M.D.[3,4]
G. P. Delaney, M.D.[3,4]
S. Vinod, M.D.[3,4]
W. Tomé, Ph.D.[6,7]

[1]Centre for Medical Radiation Physics, University of Wollongong, NSW, Australia

[2]Queen's Centre for Oncology, Hull & East Yorkshire Hospitals NHS Trust, Hull, UK

[3]Liverpool Cancer Therapy Centre and Ingham Institute, Liverpool Hospital, Liverpool, NSW, Australia

[4]South West Clinical School, University of New South Wales, NSW

[5]Institute of Medical Physics, University of Sydney, NSW

[6]Departments of Human Oncology and Medical Physics, University of Wisconsin Medical School, Madison, Wisconsin, USA

[7]Institute of Oncophysics, Albert Einstein College of Medicine of Yeshiva University, Bronx, NY, USA

*Corresponding author:
P. Metcalfe, Ph.D.
E-mail: metcalfe@uow.edu.au

Introduction

Developments in the field of radiotherapy such as intensity-modulated radiation therapy (IMRT), volumetric modulated arc therapy (VMAT) and tomotherapy have provided the means to deliver highly conformal treatments offering the promise of improved sparing of normal tissue and escalation of tumor dose. For these techniques to achieve their full potential there is an increasing need for anatomical and functional imaging to be used at the planning stage, and ideally as a verification tool throughout radiotherapy to localise disease with a high level of accuracy.

Computed tomography (CT) for imaging uses ionizing x-rays, and hence carries some stochastic increased risk in induction of a second primary malignancy from the ionizing radiation (1). While the risk of a single CT scan for planning is extremely small this risk is increased with repeat CT imaging in such scenarios as adaptive replanning in the radiotherapy setting and with prolonged survival. Because MRI does not rely on ionizing radiation for imaging, there is no increased potential induction of secondary primary malignancies associated with its use.

Magnetic resonance imaging (MRI) is a non-ionising technique that uses a strong magnetic field to provide high-resolution anatomical information with excellent soft-tissue contrast. By using specific MRI techniques, functional information such as tumor perfusion vascular permeability, extracellular space tortuosity, metabolic status and hypoxia can also be obtained (2).

Development of MRI-Cobalt (ViewRay™) and MRI-linac prototypes is underway. It is envisaged these will enable MRI to be used for on-line image-guided radiation therapy (IGRT) (3, 4). The production of combined MRI-linacs is not trivial. Apart from the engineering challenges of RF perturbation from the linac, there is the requirement to account for various electron-beam perturbation effects that affect dose at regions of air and lung-tissue interface (5). There has also been a feasibility study into the use of MRI in image guidance for proton machines (6).

The focus of this review article is to provide some insight into the current role of MRI in radiation-therapy treatment planning. A future enhancement of this role is explored by examining clinical trials data of various cancer-treatment sites, sequences and analysis methods, such as functional MRI, that are currently applied to cancer management.

Methods

Current literature has been reviewed using Medline and Google scholar to establish the MRI sequences that have been considered for radiotherapy treatment planning purposes, and MRI sequences that show potential for future use. The use of MRI for radiation therapy treatment planning purposes has been considered across all clinical sites, with a more detailed review of the use of MRI in radiotherapy treatment planning for six clinical sites.

The first section of the results presents definitions and basic acquisition details for standard MRI sequences and imaging analysis methods used for, or considered for future use in, radiotherapy treatment planning. This provides a series of definitions that help with the discussion about sequences and analysis methods used in current MRI clinical practice and trials, and includes concepts behind functional techniques such as dynamic contrast enhanced (DCE), diffusion-weighted (DW) MRI sequences and magnetic resonance spectroscopic imaging (MRSI).

The second section of the results discusses significant applications of MR in terms of the following treatment sites: brain, head and neck, breast, lung, prostate and cervix

Results

MRI sequences that have been considered for, or show potential for use in, radiotherapy treatment planning.

The most commonly used of the MR-visible nuclei is the hydrogen proton, which produces the strongest signal and is abundant in the body (primarily as water and fat). By changing the sequence parameters, MR images exploit the differences in either "longitudinal" (T1) or "transverse" (T2) relaxation times of fat and water, producing large variations in contrast.

In general, T1-weighted images are considered best for gross structural information (anatomy) and T2-weighted images for biological characteristics that may aid with pathology information. However, while extremely useful in many clinical applications and for diagnosis, neither of these imaging methods provides sensitive or specific diagnosis and localization of either prostate or breast cancer (7, 8). This is because the tissue properties that give rise to differences in T1 and T2 are not closely related to the tissue structural features that define cancer. This shortcoming also applies to CT, which reconstructs images from attenuation maps of x-ray projections, and hence essentially tracks tissue-density changes (9, 10). There is, however, more potential to enhance MRI sequences, providing functional data to ascertain more clinical information such as tumor response than possible with CT. Some of the more exciting advanced techniques are outlined in this paper; many fall within the realm of so called "functional MRI". Hence this term has been adopted (and used here) to describe any MRI technique capable

of demonstrating information in addition to the anatomical images more routinely acquired (11-13). As a general description, functional MRI is used to define techniques that probe the status of the tumor itself. Some of the most relevant examples for radiotherapy are described briefly below.

Dynamic Contrast Enhanced MRI (DCE-MRI)

DCE-MRI is performed by sequential imaging following the injection of a suitable paramagnetic contrast agent (usually some gadolinium-based chelate). Fast gradient-echo sequences are used to image each slice as fast as possible with temporal resolutions of 2-10s for 2D techniques and around 30s for 3D volumetric data. By using T2* images, data on tissue perfusion and blood volume can be extracted. By using sequences sensitive to the presence of contrast medium, T1 methods can be used to evaluate the extravascular extracellular space. Information on micro-vessel perfusion, permeability and extracellular leakage space can also be obtained. The vast amount of imaging data produced by these methods may be viewed in a cine format either with or without pre-contrast subtraction. Regions-of-interest may be interrogated to produce enhancement-time curves with malignant tumors demonstrating a rapid wash-in and wash-out of contrast. Alternatively simple empirical measures such as peak enhancement or wash-in rate can be produced on a pixel-by-pixel basis to provide parameter maps. More sophisticated models look to establish real physiological parameters from these datasets (14). DCE-MRI has been shown to have diagnostic value in various tumors, and correlates with the therapy effect of standard chemotherapy and radiotherapy (2).

Diffusion-Weighted MRI (DW-MRI)

DW-MRI scan sequences produce image contrast that depends on differences in tissue-water mobility. Two equally large, opposing gradient pulses in the diffusion sequence make the signal intensity dependent on the movement of water molecules. The first gradient pulse induces a phase shift of water molecules, followed by incomplete rephasing after the second gradient pulse, with the phase difference depending on the mobility of the water molecules. Incomplete rephasing of water molecules is less pronounced in hypercellular tissue, characterized by less signal loss; rephasing is more pronounced in hypo-cellular tissue, which shows increased signal loss (15). The apparent diffusion coefficient (ADC), in units mm^2/s, is the quantitative parameter used for the assessment of water diffusion through tissue. The term apparent reflects the concept that the measurement is subject to other factors not just water mobility. The sensitivity of the gradient scheme is defined by its "*b*-value": by acquiring at least two images with different *b* values (usually $b = 0$ and $b = 1000 \, s \, mm^{-2}$) the ADC can be measured directly. The mean ADC values in the benign and malignant Head and Neck lesions have been observed as 1.51×10^{-3} mm^2/s and 1.07×10^{-3} mm^2/s, respectively (16).

In biologic tissues, the movement of water molecules is restricted because their motion is modified and limited by interactions with cell membranes and macromolecules. There is an inverse correlation between the degree to which the motion of the water is restricted and the tissue cellularity. This inverse correlation also applies to the integrity of the cell membrane. Hence in a tumor with high cellularity, the motion of water molecules is more restricted. On the other hand, when a tumor has a high glandular component or has significant necrosis, there is less restriction of motion. In general, treatments inducing apoptosis (*e.g.*, chemotherapy) result in increased ADC values due to cell swelling, tumor lysis and necrosis (2).

In adenocarcinoma of the breast and prostate, for example, cancer development is characterized by the proliferation of epithelial cells and the loss of normal tissue architecture. An imaging method that generates contrast based on microscopic tissue structural properties would be expected to provide cancer detection and staging, such that the contrast can be made to reflect the structures that define pathology. DW-MRI is an ideal candidate for this purpose because the free diffusion of water in tissue is known to be constrained by cellular structures and cell walls. This property has been used extensively in the study of neural tissue; the concept also been reported in cohort studies of head and neck cancer cases, but has had only limited clinical application to diseases of glandular tissue such as breast and prostate (15). Pathologic prostate samples have also been examined at very high resolution (nominally 40 microns) in vitro in high field MR (16 T) and the lymphatic structures may be a confounding factor for ADC analysis at typical clinical voxel resolutions (17).

Diffusion-weighted imaging is probably the most useful new tool in tumor response, and cohort studies show its potential in providing evidence of tumor recurrence. One of the challenges with these sequences is that image-distortion artifacts are apparent in some of these sequences. Thus, defining regions of tumor burden may need some form of deformable registration to other MRI sequenced images or CT images if these potential volumes of recurrence are to be targeted with extra radiation treatment doses to selective intra-GTV regions by dose painting (18) or risk-adaptive boosting (19).

Magnetic Resonance Spectroscopic Imaging (MRSI)

MR spectroscopy provides chemical information about tissue metabolites, commonly using the MR visible nuclei of hydrogen (^{1}H), phosphorus 31 (^{31}P), fluorine 19 (^{19}F)

or carbon 13 (^{13}C). Each specific nucleus exhibits a slight change in processional frequency that depends on its chemical environment. Specifically, variations in the electron shielding of different molecules alter the magnetic field and resonant frequency (the chemical shift). An MR spectrum is a kind of molecular fingerprint and may contain many peaks at specific frequencies (or chemical shifts), one for each chemically distinguishable site or group in a given metabolite or for specific sites in a variety of metabolites (2).

The technique can be extended to MRSI, whereby spectra are acquired from multiple contiguous volumes (voxels), and peak areas or ratios are displayed with a color wash overlying the anatomy to provide a metabolic map. The small concentrations of metabolites necessitate the use of large voxels, and resolution can be as much as an order of magnitude poorer than in conventional imaging. Nevertheless, MRSI has been found to be useful in quantifying brain function and brain-related cancerous tumors where the relative amount of NAA to choline (related to cell turnover) is informative. In the prostate, the ratio of citrate to choline or choline+creatine is used in a similar manner.

Lactate has been found to be indicative of hypoxia, and could therefore be used to mark out radio resistance. However Lactate can not currently be analysed accurately *in vivo* for prostate cancer. This biomarker can only currently be visualized in prostate pathology samples *ex-vivo* at higher field strengths. Lactate has been successfully identified from lipids in head and neck and brain tumors with recent *in vivo* patient techniques (20).

Some degree of expertise is required to interpret the data, and the incorporation of this information into the planning system is still in its infancy. Another challenge when imaging hypoxic regions is that hypoxic zones may be chronic or acute, and may change position over time. As this article does not focus on MRSI in great detail, the reader is guided to an excellent review on its use in brain, breast and prostate cancer (21).

Fast Sequences

MRI is an inherently slow technique compared to CT, requiring numerous applications of imaging gradients to obtain the desired "*k*-space" data; the faster these gradients can be switched on and off, the faster the scan can be acquired. T2-weighted spin-echo sequences, with long repetition times (TR), are inherently slower than T1-weighted gradient echoes, which are often used as the basis for rapid imaging (22). Both types of sequences can be performed using segmented and partial *k*-space strategies to improve imaging speed. Single-shot techniques, like eco planar imaging (EPI), apply all the gradient steps very rapidly in one single repetition. However, nerve stimulation provides a physiological limit to gradient speed and has necessitated other developments with the aim of faster imaging. In the last several years parallel imaging has become available on all commercial systems: it substitutes some of the gradient steps with information provided from RF coil sensitivity profiles. All these techniques have combined to allow MRI to acquire sub-second images, and have opened the technique up to a number of challenging areas. These fast sequences may be critical to future IGRT applications of MRI.

Hyperpolarization

The sensitivity of MRI and MRSI can be increased 1,000 to 10,000 times using hyperpolarization, whereby a sample containing nuclei that had their spin population temporarily driven to a very high degree of polarization is introduced into the body. Procedures to probe pathological defects have been optimized for two noble-gas isotopes that can be inhaled into the human lung: helium 3 (^{3}He) and xenon 129 (^{129}Xe). An optical (laser) pumping technique is used to hyperpolarize the orbital electrons of alkali metal atoms, *e.g.,* rubidium, through angular-momentum transfer. This polarization is then transferred to the nuclear spin system of the gas through direct atomic contact. Once mixed with oxygen in the lung, the half-life of the hyperpolarised signal is extremely short, meaning the fast imaging strategies previously described become of vital importance.

A number of lung-function medical conditions can benefit from functional imaging using ^{3}He MRI, as reviewed by Fain *et al.* (23). For example, these images have been used for conformal avoidance of lung tissue that is the most active in gas exchange, as shown by ^{3}He scans. Figure 1 shows such a high-activity region of ^{3}He uptake in orange (right) fused to an MRI proton density scan image (left). The orange region could then potentially be set as a threshold level, then contoured for conformal avoidance during the radiotherapy treatment planning process (24). Xenon has the added advantage that its transport into the lung tissue can be detected as a chemical shift change with MRSI.

Hyperpolarization also has a role to play in ^{13}C spectroscopy in the study of tumor metabolism, although this still remains a research tool. Its low natural abundance means a ^{13}C-labeled tracer can be introduced into the body with little baseline contamination. Its low sensitivity can be increased dramatically with techniques such as dynamic nuclear polarization (DNP) and parahydrogen induced polarization (PHIP) (25, 26). Unlike PET tracers, which are mainly analogues of metabolites, ^{13}C tracers undergo metabolic changes and can be studied as they alter the appearance of the MR spectrum.
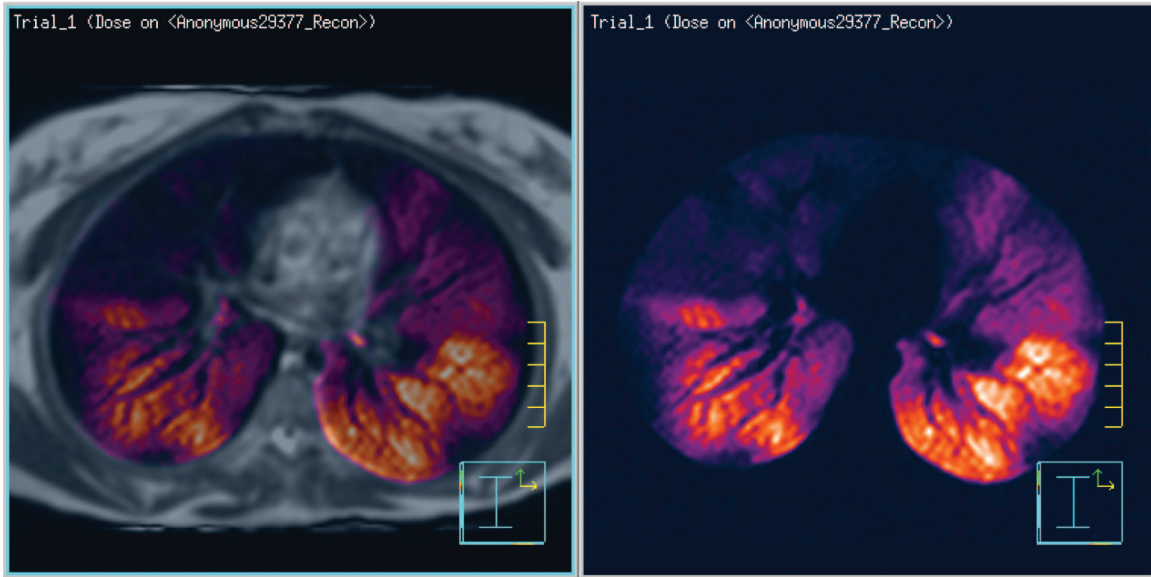
Figure 1: ^{3}He polarization image showing polarized MR helium 3 diffusion scan (right) fused on a proton-density-weighted MR scan (left). These active zones would be the regions of conformal avoidance, defined as low-dose objectives during the radiotherapy treatment planning process.

### Site-specific Use of MRI in Radiotherapy Treatment Planning

This section reviews clinical trials of sites for which various MRI sequences and analysis methods have been useful in cancer management. The sites selected for review cover brain, head and neck, breast, lung, prostate and cervix, and are not intended to be exhaustive.

Brain

Owing to its small size and central location within the magnet, the brain is one of the easiest organs to image well.

MRI is well established as the superior imaging modality for diagnostic purposes when assessing the brain. In the brain, MRI often provides better visualization of tumor and normal tissue than CT, and hence the target volume for high-precision intracranial radiotherapy is commonly delineated directly on MRI studies (Figure 2). It can be imaged in standard diagnostic RF coils usually in the treatment position, and its registration to CT is trivial even with differences in position.

The brain was the first site where MRI was routinely used in treatment planning. Routine clinical use of MRI in the treatment-planning process of fractionated radiotherapy (RT),
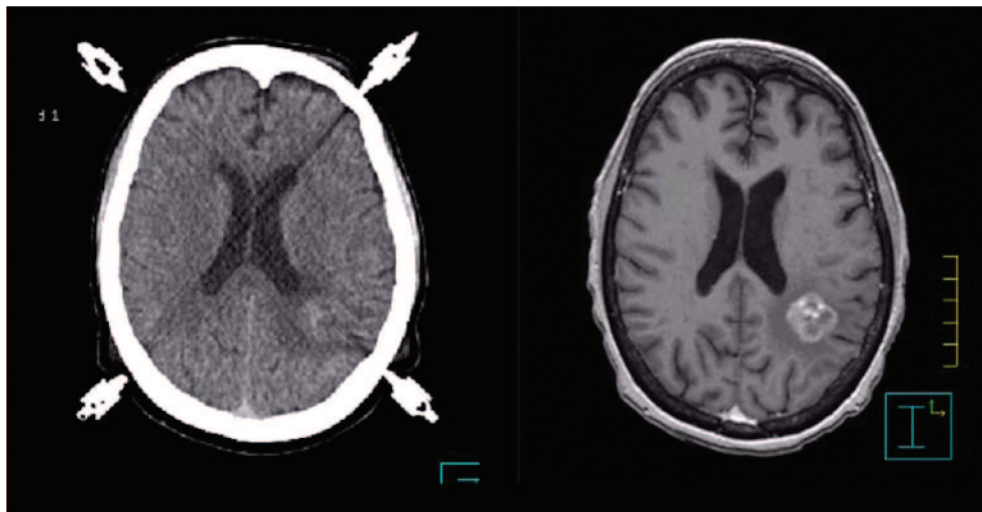

Figure 2: CT (left) co-registered with a T1-3D-SPGR MRI image set (right). The difference in tumor visualization can be clearly appreciated.

fractionated stereotactic radiotherapy (FSRT), stereotactic radiosurgery (SRS) and functional radiosurgery (FSRS) has been found to be a useful tool in brain tumors.

The treatment target for a patient having a high-grade glioma can be determined from both a contrast-enhanced T1-weighted high-resolution 3D spoiled-gradient (SPGR) image as well as either a standard T2 MR image (27) or a fast fluid-attenuated inversion recovery (FLAIR) image (28). The T1-weighted high-resolution 3D SPGR is used to define the gross visible disease, which is the region of the blood-brain barrier breakdown, while the clinical target volume is defined using the T2-weighted image series on which the extent of the oedema thought to harbor microscopic disease is delineated. On the other hand, for benign lesions as well as brain metastases that do not invade the normal brain parenchyma, a contrast-enhanced T1-weighted 3D SPGR is sufficient for target definition in FSRT and SRS (29).

In the treatment of arteriovenous malformations (AVMs), magnetic resonance angiography (MRA) is employed for the definition of the nidus, which most of the time cannot be clearly appreciated on T1-weighted MR images (30). Moreover, in the treatment of trigeminal neuralgia using functional stereotactic radiosurgery, 3D fast imaging employing steady-state acquisition (FIESTA) MRI is employed for visualization and targeting of the involved trigeminal nerve 4 mm from the root entry zone. Since this imaging technique has a significant T2-weighting, the cerebral spinal fluid around the brain stem luminates while normal brain and cranial nerves appear almost black. This allows delineation of the involved trigeminal nerve root as it emanates from the brainstem (31) (Figure 3).
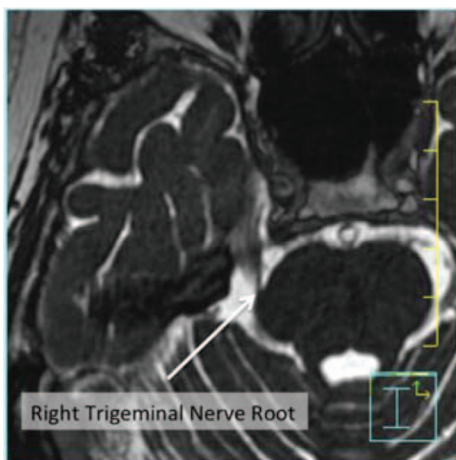
Figure 3: Visualization of the right trigeminal nerve root using FIESTA MR imaging. The arrow points to the right trigeminal nerve root.

To explore the potential to reliably compare intra- and post-treatment images with pre-treatment images on a voxel-by-voxel basis, *i.e.* using voxel-based functional diffusion maps at various time points to predict the response of brain metastases to whole-brain radiotherapy, a diffusion-mapping technique has been developed at the University of Wisconsin that allows the reliable comparison of intra- and post-treatment images with pre-treatment images on a voxel-by-voxel basis (32, 33).

An example for one patient is shown in Figure 4; green points on the graph indicate no change in ADC for a voxel from the baseline to the assessment time point, red points indicate that the ADC has increased at the assessment time point as compared to the baseline and blue points indicate that the ADC has decreased from the baseline. An increase in ADC (red points) in a voxel indicates increased diffusion distance of the water molecules, and hence a decrease in cell density, which could indicate that the volume is responding to therapy. In the same way, no change in ADC (green points) could indicate no response to therapy, and a decrease in ADC (blue points) indicates a decreased diffusion distance of water molecules, and hence an increase in cell density, which could indicate a proliferating volume of cells during therapy.

Another brain technique can be used to adopt a conformal avoidance strategy. Functional MRI (fMRI) has been incorporated into the TPS to consider defining various functional organs at risk (fOAR). Work has also looked at the robustness of this technique in terms of recommending planning margins of uncertainty (11). The benefits of including such information remain to be proven, but results show that several primary functional areas can be included in the planning prescription without any adverse changes to the planning target volume (PTV) coverage (12, 34).

In the setting of brain metastases, investigation on the utility of DW-MRI for assessing response to therapy has been limited. Goldman *et al.* have studied diffusion-weighted MRI in 15 patients who underwent gamma-knife radiosurgery for brain metastases, and demonstrated the potential for early changes in mean ADC to predict therapeutic response (35). However, their assessment of changes in mean ADC was obtained by averaging over an entire metastatic lesion, not by using a voxel-by-voxel approach. One potential disadvantage of mean ADC is that different areas of tumor with increasing and decreasing changes in diffusion could cancel out, such that there would be no observed change in overall mean ADC, thus decreasing sensitivity.

Some MRS data can be incorporated into TPS. Some degree of expertise is required in incorporation into planning as use of this data is still in its infancy (36, 37)
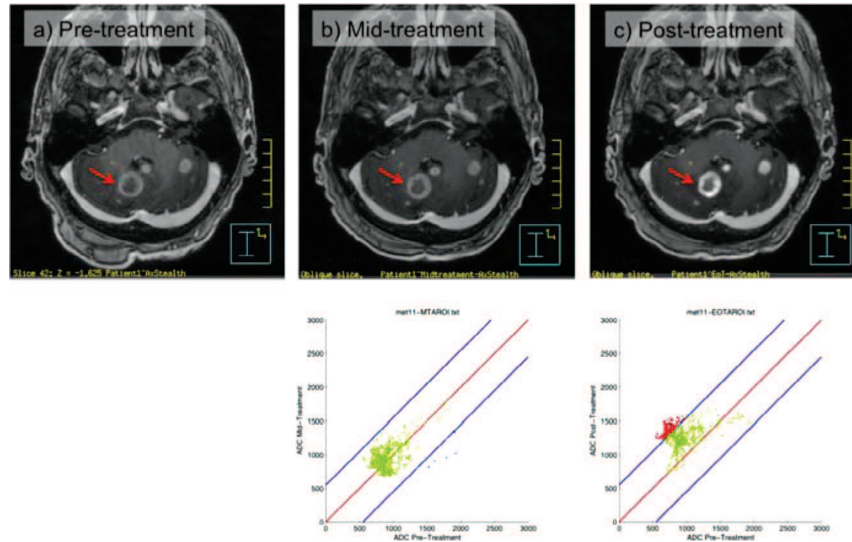
Figure 4: MR images at various stages of radiotherapy: (**A**) before radiotherapy, (**B**) mid-treatment and (**C**) post-treatment. The graphs in B and C show the voxel-by-voxel ADC values changing as determined during ADC image analysis on MRI. Green points on the graph indicate no change in ADC for a voxel from the baseline to the assessment time point, while red points indicate that the ADC in a voxel has increased compared to the baseline, and blue points indicate that it has decreased compared to the baseline.

Head and Neck

Historically, the sensitivity of FDG PET was generally reported as higher than conventional MRI scans for detecting lymphogenic metastesis in head and neck cancer patients. For example, Braams *et al.* (38) reported for FDG PET a sensitivity of 91% and specificity of 88%. In contrast, a sensitivity of 36% and a specificity of 94% were calculated for MRI using T1- and T2-weighted scans.

However, with the advent of specialised RF coils for imaging in treatment shells, the use of advanced signal-hungry

MRI sequences has improved markedly. With specialised RF coils patients can also undergo MRI in the treatment position, improving the accuracy of any image registration. Figure 5 shows a typical treatment coil for head and neck MRI scanning.

Vandecaveye *et al.* (15) scanned a 26-patient cohort with persistent or recurrent head and neck squamous cell carcinoma (HNSCC). Compared with histopathologic findings, they showed a sensitivity and specificity of around 95% using ADC analysis. In comparison T1- and T2-weighted MRI scans of b0 (s/mm^2) images gave a specificity and sensitivity

Figure 5: Photograph showing the set-up for head & neck planning on a wide-bore MRI scanner. A flat tabletop is used in conjunction with the standard thermoplastic immobilization shell. Two dedicated RF surface-coil arrays are placed laterally around the shell to enable high-quality imaging in the treatment position.

of approximately 65%, while b1000 images scored a sensitivity and specificity of about 72%. When compared with computed tomography, TSE-MRI and FDG-PET, the DW-MRI sequence analysis yielded the highest sensitivity and specificity with fewer false-positive results in persistent primary site abnormalities and in persistent adenopathies, and aided in the detection of nodal metastases that were indicated as smaller than 1 cm diameter.

There can be advantages in registering and overlaying FDG PET images with MRI or CT contours. Nishioka *et al.* (39) showed that the PET scans could be used to confirm whether parotid sparing was appropriate by analysing uptake. The PET also confirmed that the total number of positive nodes in the 21 patients was increased from 28 by physical examination coupled with CT/MRI to 39 by the image fusion of the PET scans with the MRI/CT. The recent introduction of combined PET-MRI gantries represent a new exciting area of clinical research into analysing the potential advantages of combining these imaging data sets, which will have similar acquisition time stamps.
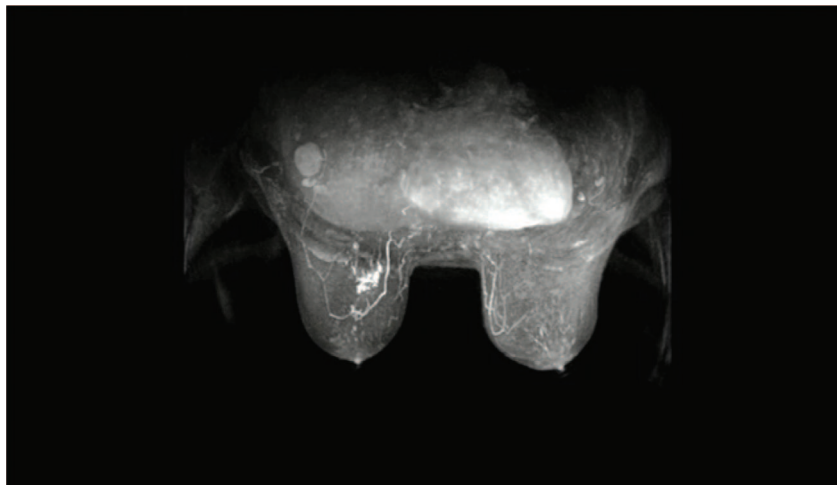
Breast

Breast abnormalities are visible on MRI using both non-contrast and contrast-enhanced MRI scans. MRI has been shown to have greater sensitivity than mammography for assessment of extent of breast cancer under certain clinical conditions (40-48), making MRI a potentially interesting tool in the appropriate planning of radiotherapy.

The purpose of standard post-operative tangential radiotherapy following wide local excision for early breast cancer is to treat the remaining breast volume. However, the breast volume is poorly defined by CT (49), and attempts are often made to supplement identification of breast tissue by palpation and delineating on the patient with radio-opaque catheters when undergoing CT scanning. Giezen *et al.* (50) performed an exploratory study of MRI versus CT for delineation of breast volume for the purpose of radiotherapy planning. In a small study of 15 patients and four volume delineators, it was observed that MRI detected breast glandular tissue beyond that identified by CT scanning, especially in the cranial direction, and that this tissue may be conventionally missed geographically if CT planning is relied on to delineate volume. The clinical uncertainty is whether this "missed" tissue is seen in a larger cohort of patients and observers. The current very good local control rates for breast conservation radiotherapy in general do pose the question of whether these differences in volume make any difference to clinical outcome. Recurrence rates are still significant, especially in younger patients (51) who have denser breasts, and this may be a cohort that benefit most from better volume delineation. Their findings therefore warrant further examination. Figure 6 gives an example of a typical breast image taken of a patient lying prone in breast coils.

One difficulty for MRI planning in the breast is the contradictory patient set-ups: treatment is performed in the supine position, whereas optimum imaging is performed with the patient lying prone and the breasts suspended in separate wells of the RF coil. Although MRI of sufficient quality can be obtained in the supine position using a body coil array, the breast tissue is then positioned further from the isocenter, causing issues with geometrical accuracy (52).

An emerging trend is to treat some patients with favourable histology with partial breast radiotherapy directed to the site of the surgery only. Clinical studies are currently underway. Kirby *et al.* (53) assessed breast-cancer patients positioned

Figure 6:   MR image of breast showing irregularities (anatomical right breast). Most breast images are obtained using breast surface coils to reduce the signal-to-noise ratio, and the patient is usually positioned prone in the coils. This image is courtesy of the Aroura web site (www.Aroura.com).

prone to determine the value of MRI and CT for planning partial breast irradiation (PBI) to the tumor bed (TB). They found that TB volumes delineated using fused MR and CT/clip data were discordant to those delineated using CT/clips alone. However, resulting clinical and planning-target volumes were sufficiently concordant to ensure adequate coverage of the target volume using the CT-based tangential treatment fields in 26 of 30 cases, suggesting that the use of MRI for most cases did not lead to a substantial change in treatment volume. Two of the 30 cases showed inadequate coverage due to discordance between volumes, both inferiorly. Another two of the 30 cases showed that inadequate coverage was related to the target volumes being located at the peripheries of breast tissue, where coverage is difficult due to the complex 3D shape of breast tissue. This study suggests that MRI may only have a limited role to play in delineation of the TB post-operatively when CT data with clips defining the TB is available.

However, there may be a role in the future for defining the TB pre-operatively using MRI as the imaging modality of choice. The study reported by Schmitz *et al*. (54) compares breast MRI with pathology to assess treatment margins in 62 patients. While the MRI-estimated GTV showed close concordance with the pathologic samples, these samples also showed significant spread of occult pathology. The findings report that for MRI-guided minimally invasive therapy, typical treatment margins of 10 mm around the MRI-GTV may not incorporate occult disease in 52% of patients. When surgery achieves a 10 mm tumor-free margin around the MRI-GTV, radiotherapy to the TB may require clinical target volume margins of greater than 10 mm in up to 25% of the patients. The outcome from breast-conservation studies does not suggest such a high recurrence rate as might be predicted by these figures, but may perhaps identify patients who might be at greater risk of recurrence. Correlation of tumor extent with breast recurrence rates will be required.

Ultra small particles of iron oxides can act as a negative contrast agent and are taken up by normal tissue on T2* weighted sequences. Their sensitivity and specificity for detecting nodal metastases is high (55). These allow detection of micrometastases in the nodes as small as 2 mm in diameter. New promising agents such as ferumoxytol are under investigations for FDA approval.
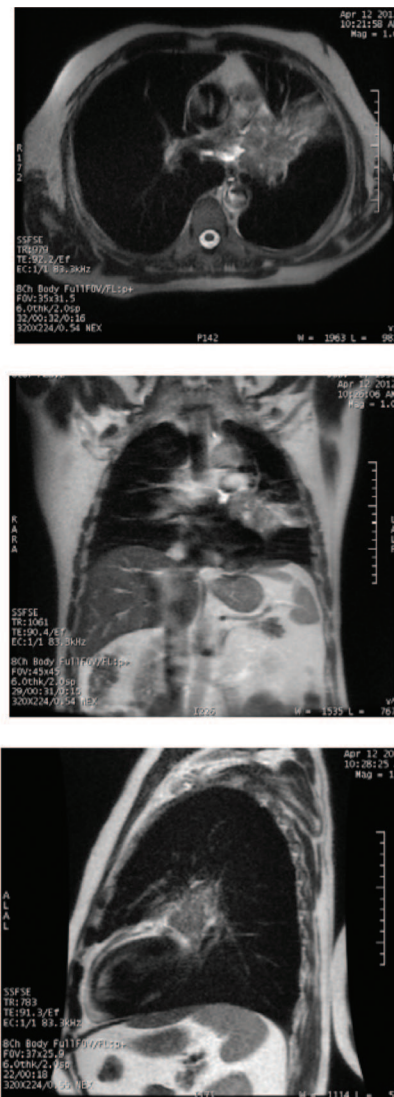
Lung

CT scans with the addition of FDG PET is the standard of care for diagnosis of lung cancer; however, there is poor distinction between structures with similar electron densities, making it difficult to differentiate lung cancers from surrounding lung collapse, consolidation or effusion. MRI can enable differentiation of these situations through improved soft-tissue contrast. MRI scans can be undertaken in a similar position to that used for radiotherapy treatment.

Figure 7 shows a T2-weighted single-shot fast-spin echo (SSFSE) image of a small-cell lung cancer. There is excellent differentiation between mediastinum and tumor mass, while the boundary between tumor and consolidation is less clear.

Of particular interest for defining radiotherapy treatment volumes for lung cancer is the ability to accurately determine lung-cancer motion. MRI is becoming an increasingly attractive modality to image this motion. Parallel imaging

Figure 7: Axial, coronal and sagittal plane of a T2-weighted single-shot fast-spin echo image of a small-cell lung cancer for a 64-year-old male with T4 N2 M0 disease. There is excellent differentiation between the mediastinum and tumor mass, although the boundary between the tumor and the consolidation is unclear. (Images done on 1.5T GE scanner, with inspiration breath-hold.)

techniques improve both spatial and temporal resolution. There are two particular sequences useful in imaging motion: fast low-angle shot (FLASH) sequences and true fast imaging with steady-state precession (TrueFISP) sequences. Plathow *et al.* (56) investigated these two imaging sequences to quantify tumor mobility in 20 patients with Stage I non small cell lung cancer (NSCLC). Both techniques showed regular, synchronous diaphragm and chest-wall motion of diagnostic quality. The TrueFISP sequence acquired three images per second, allowing for continuous recording during the respiratory cycle, and correlated well with the FLASH sequences, which acquired 10 images per second. There were no significant differences in measurement of tumor mobility between the techniques; however, the signal-to-noise ratio was superior for TrueFISP.

Other sequences used to image motion include a multi-slice breath-hold steady-state free-precession sequence and dynamic 3D free-breathing fast-field echo planar imaging (FFE-EPI). Blackall *et al.* (57) used these sequences to evaluate 3D geometric errors associated with respiratory motion variability in 10 volunteers and five lung-cancer patients. The protocols were optimized for each participant by adjusting the voxel size, to obtain coverage of the entire lung at the highest possible resolution while maintaining an acceptably short acquisition time. The participants were coached to help them regulate breathing. Images were acquired throughout the respiratory cycle and registered to demonstrate motion using different models. Respiratory-motion models based on rapidly acquired free-breathing MRI data showed reasonably good levels of inter-cycle reproducibility, with mean errors at the lung surface in the range of 1.7 to 3.9 mm for healthy volunteers, and 2.8 to 3.3 mm for lung-cancer patients. Inter- and intra-cycle variability were less during exhalation.

Dynamic MRI can thus be used to define a patient-specific ITV for planning of lung cancers for radiotherapy. It allows the entire lung volume to be imaged fast enough to analyse true motion and deformation over the breathing cycle, while the patient breathes freely, as occurs during radiotherapy treatment. MRI studies using TrueFISP sequences have shown that lower-lobe tumors move more than upper- or middle-lobe tumors, and that the movement of tumor-bearing lung is reduced compared to normal lungs (12, 58). The latter is also dependent on tumor diameter, with less movement seen in larger tumors (58). However, dynamic MRI of the lung is prone to artefact, which affects registration accuracy for the purposes of radiotherapy planning.

Dynamic MRI imaging of lung cancers can be used for probability density function (PDF), planning whereby the dose distribution of radiotherapy is modulated by the probability that the target occupies that location. In a study using 17 healthy volunteers and lung-cancer patients, Cai *et al.* (59) developed a technique to measure this using TrueFISP sequence. Improvement in PDF reproducibility was observed with increased imaging duration and a greater number of sampled breathing cycles. Two patient-specific imaging acquisitions were recommended to establish the reproducibility of the PDF if PDF-based treatment planning was being considered.

The current standard of 4DCT is not as accurate in determining the tumor-motion PDF. It has lower temporal resolution, particularly in detecting craniocaudal motion. The tumor-motion trajectory is measured from segments of numerous breathing cycles rather than a single breathing cycle. To take true respiratory motion into account for radiotherapy planning and treatment the entire organ needs to be imaged at high speed while the patient breathes normally. This is not possible with 4DCT. Variability in respiratory motion from one cycle to the next can be magnified in 4DCT images, leading to artefacts. It cannot image the statistically needed number of complete breathing cycles for a reproducible PDF.

There have been no definitive contouring studies comparing the delineation of lung cancer on MRI to CT or PET-CT scans. As a diagnostic tool in differentiating benign from malignant nodules, techniques such as DWI have shown similar accuracy to PET scans (60). DCE-MRI has shown some promise in differentiating between subtypes of lung cancer in inoperable cases (61). This may have an impact on determination of CTV margins and type of chemotherapy delivery in cases where histological subtype has not been determined by biopsy.

The use of MRI to avoid normal tissues in lung-cancer radiotherapy planning is an emerging area of research. This is possible with the use of inert hyperpolarized helium-3 gas, which is inhaled to demonstrate regional lung function by selective display of ventilated air spaces. Non-ventilated regions show up as signal voids. Bates *et al.* (62) contoured functional lung based on helium MRI on seven patients with Stage III NSCLC (14). Two IMRT plans were created: the first to minimise total lung volume receiving ⩾20 Gy (V20) and the second to minimise functional lung volume receiving ⩾20 Gy (fV20). In all patients, the addition of functional information reduced both V20 and fV20 without compromising target coverage. The median reduction in V20 was 1.5% and fV20 2.7%; however, mean lung dose was not significantly different. Larger reductions were seen if the non-functional lung was >25% of total lung volume. Similarly, Ireland *et al.* (63) observed a median reduction of 1.6% in V20 and 3.1% in fV20 in six plans. The greatest benefit was seen if functional lung lay in the path of the beam and could therefore be spared by alternative beam arrangements.

MRI scans can be used to evaluate changes in lung tumors and normal tissue response during a course of radiotherapy. Yankelevitz *et al.* (64) performed 0.6T MRI scans before, during and after radiotherapy in 10 patients. After 20 Gy tumors decreased by 38%, and after 40 Gy by 64%. All patients showed increased signal intensity in normal lung tissue during radiotherapy but without clinical evidence of radiation pneumonitis. This increased up to six months after radiotherapy before decreasing. Other authors have noted changes in tumor vascular permeability on DCE-MRI during treatment, reflecting changes in microvascular structure (65). MRI has the potential to allow adaptive radiotherapy planning in response to changes during treatment.

Finally, MRI may be used as a prognostic tool for treatment outcomes. Ohno *et al.* (66) performed post-treatment DCE-MRI scans in 114 evaluated patients who had chemoradiotherapy for Stage III NSCLC. A breath-hold technique at end-inspiration was used. Patients were divided into two groups for analysis: those with local control and those with local failure. Signal-intensity time curves of the tumor and normal lung were created and evaluated. Survival was compared above and below an adopted threshold value for dynamic MRI index. An 11-month difference in survival was noted between the two groups. However this has not been compared to other imaging such as PET scans.

Prostate

The use of MRI for diagnosis of prostate cancer is not currently standard; however, MRI is recognised as a superior imaging modality in defining the prostate volume accurately, and, with advanced techniques such as MRSI, has the ability to distinguish between the cancer volume and normal prostate tissues.

Prostate scans may be acquired in the treatment position using a flat tabletop and a posterior RF coil placed underneath it without too much loss of quality (67). A support over the body can be used to avoid compression from the anterior RF coil if required. Any residual distortion at the skin surface can be largely ignored or a smaller FOV acquired and matched to sufficient bony anatomy in the CT.

A clear indication for MRI is in cases of bilateral hip replacement; Rosewall *et al.* (68) showed that smaller prostate volumes were delineated on the MRI compared to CT, which is adversely effected by high Z artefacts. In contrast, there is no effect from the susceptibility artefacts on the MRI, which are confined to within the prostheses.

For gold-seed localization as used in image guidance for intact prostate radiotherapy, the MRI exam sequence may include a gradient echo-based sequence that improves the visualization of the markers by virtue of susceptibility artefacts.

Khoo *et al.* (69) undertook a five-patient cohort study to compare contour segmentation of structures in the prostate region. Using a subjective scoring system, they concluded that MRI was superior to CT when observers were segmenting the prostate apex and rectum. The FLASH 3D sequence showed the best images, as no volume averaging was involved with this sequence.

Haider *et al.* (70) studied 33 prostate patients with suspected relapse after external beam radiotherapy. They compared T2-weighted with dynamic contrast enhanced (DCE) MRI scans, concluding that DCE-MRI performed better than T2-weighted imaging in the detection and localization of prostate cancer in the peripheral zone after EBRT. This finding may be helpful in the planning of salvage treatments.

McLaughlin *et al.* (71) explored the premise that vessels involved in erectile function – the corpus cavernosum (CC) and the internal pudendal artery (IPA) – may be affected by radiation, based on proven radiation effects to other vasculature structures in the body. They studied 25 patients undergoing radiotherapy, 10 external beam and 15 brachytherapy patients. MRI T2 sequences (axial, coronal and sagittal) were obtained with a pelvic coil. Of these patients, 10 were entered on a vessel-sparing protocol and underwent treatment-planning CT. In addition, a non-contrast MRI angiogram was obtained to define the IPA. The proximal CC was clearly defined on axial and coronal T2 MRI. Hence they showed the potential of MRI to visualize the prostate and erectile structures. They registered the MRI data sets by mutual information and created radiotherapy treatment plans that allowed dose limitation to the critical erectile tissues (the CC and IPA) without compromising target coverage. While these structures are visible with MR angiography, the researchers suggested that coronal images using conventional MRI T2 sequences provide sufficient detail of the outline and position of these vessels for conformal avoidance in radiotherapy. They predicted that it erectile vessel-sparing radiotherapy may have as favourable an impact on sexual potency after radiation as nerve-sparing prostatectomy.

McLaughlin *et al.* (71) also includes useful data on distances from the prostate apex to the penile bulb. While the mean range in their sample was 1.45 cm, they observed ranges in distance between these structures of between 0.7 and 2.1 cm. This suggests that the standard distance of 1.5 cm used with CT images may sometimes over- or underestimate distance from the apex to the vascular structures. They suggested that the use of this rule would have underestimated the distance in one half of their patient cohort, potentially leading to marginal miss. The prostate

volume would have been overestimated in the other half of their patients, limiting the degree to which erectile tissue was spared in these patients.

The argument for MR images in combination with CT for prostate radiotherapy treatment planning is compelling. However, issues remain for some of the functional techniques previously described to be used in treating the prostate. The requirement of sufficient signal-to-noise in MRSI for example, usually demands the use of endorectal receiver coils, which distort the prostate compared to its position on CT acquisition. Remedies to this include higher field strength and/or less invasive coil designs.

The evolution of multiparametric combinations of MRI sequence information, for example combining information from T2w, DCE, DW $+/-$ MRS is rapidly growing in prostate cancer detection and mapping. It increases the power of MRI over each single sequence. This may be of value in the context of radiotherapy-planning. Moreover, preliminary data on hybrid PET/MRI suggests that Choline/ADC maps could more accurately predict tumor staging and mapping. Multimodal imaging or multiparametric MRI could play a major role in the context of focal therapies or focal dose escalation (72).

Blood oxygenation can be monitored non invasively with MRI potentially providing information regarding tumour hypoxia. Blood oxygen level dependent (BOLD) sequence studies have shown a direct correlation between measurements of oxygen using an Eppendorf electrode and R2* relaxation time. These parameter maps can highlight areas that are likely to be radioresistant and requiring a boost in dose (73).

Cervix

MRI is well established as the optimum imaging modality for cervical-cancer diagnosis in comparison to CT and clinical examination (74, 75). Challenges in determining the extent of cervical cancer are in detecting stromal invasion (74, 75) and establishing lymph-node status. Detection of lymph-node invasion is currently most accurate with FDG-PET imaging. However, the accuracy of MRI has been improved with ultrasmall superparamagnetic iron oxide particles that are lymph-node specific contrast agents (76); future research may improve this further.

Use of MRI for radiotherapy treatment planning, monitoring of tumor response over the course of treatment and assessment of relapse following treatment has been investigated for over a decade. MRI is considered the imaging modality of choice for radiotherapy contouring, with significant improvement in contrast between the target volume and

normal tissues (77-79). MRI has been the imaging modality of choice for radiotherapy delineation for a number of clinical trials (79).

MRI sequences for radiotherapy delineation purposes are usually T2-weighted (80-83). The choice of coil has varied throughout the literature, with details often not provided; however, when described, generally in more recent investigations (84), it was usually a body coil with phased array coils. Similarly, patient positioning is often not detailed in the literature; however, a number of studies have achieved MRI scanning positions that mimic treatment position, including a flat couch top (82, 83, 85). The significance of treatment positioning in cervix MRI scanning for radiotherapy has not been assessed. The field of view (FOV) used for cervix MRI for radiotherapy purposes also varied, ranging from covering only the target and surrounding nearby regions (83) to encompassing the majority of the patient volume (84).

A number of other MRI sequences have been considered for the purpose of radiotherapy target volume definition and treatment response assessment, including T1-weighted sequences with and without fat suppression (81, 82, 86). Recently the use of diffusion-weighted imaging and ADC values has been investigated as a potential tool for predicting and monitoring treatment response (84, 87). Although use of ADC values for determining patients likely to respond well to radiotherapy has not yet been well established, early work is promising and warrants further investigation.

Following guidelines published in 2006 (88), MRI is being increasingly used in image-guided brachytherapy (IGBT) of the cervix. MR-compatible applicators made from materials such as titanium or plastic can be imaged safely *in vivo* with little susceptibility to artefacts using fast spin-echo based protocols. Work is currently being carried out to improve the visualization of these applicators on MRI using short or even ultrashort TE sequences.

Discussion

Use of MRI for radiotherapy treatment planning is well established for many treatment sites such as brain and head and neck, with its use in many others under investigation. There is a growing body of literature considering the use of MRI for radiotherapy treatment planning. As noted in section one of the results, a large and growing number of MRI sequences have been considered for the purposes of radiotherapy treatment planning. T1 and T2 scans are commonly used in many treatment sites. The use of DWI is showing promise in a number of clinical areas for establishing nodal involvement, and thus target volume, as well as for considering response assessment.

MRI has a proven track record in brain function studies. MR sequences in the brain aid in the diagnosis and staging of brain tumors (*e.g.,* glioma). Early studies show a correlation between tumor activity and DW images using fDM analysis methods. In some non-malignant diagnosis such as AVM and the trigeminal nerve in Neuralgia patients, specialized MR techniques (*e.g.,* MR angiography) have been used to provide exquisite targeting information for stereotactic radiosurgery applications.

MRI has been used in combination with PET scan and CT in head and neck treatment. Standard MRI techniques show the soft-tissue boundaries in this region, while PET has been effectively used to track regions of high activity that have high specificity to potential nodal involvement. DW-MRI using ADC methods shows promise in differentiating regions of tumor recurrence. There is a very high correlation in specificity and sensitivity when compared with pathological samples.

MRI has shown the potential to provide a more accurate picture of the GTV, compared with current methods such as CT. When combined with pathological analysis, surprisingly large treatment margins are sometimes required. One study has found that when surgery achieves a 10 mm tumor-free margin around the MRI-GTV, radiotherapy to the tumor bed may require clinical target-volume margins of greater than 10 mm in up to 25% of patients (54).

The future use of MRI may have an impact on discerning which clinical stages are suitable for partial breast irradiation techniques. The use of MR seems to indicate more regions of abnormality post-surgery and prior to other interventions. This may indeed have a major impact on cancer management into the future. It is not clear yet that there is an MRI technique that can discern breast tissue from other tissue. But it does seem clear that breast anomalies in and around the excised tumor bed are highlighted with subsequent MRI imaging.

MRI has huge potential in radiotherapy treatment of lung cancer. It has a role in diagnosis, tumor delineation, measurement of motion and identifying functional normal tissues to avoid. It can also be used during radiotherapy to allow potential treatment adaptation in response to changes occurring in the lung tumor and surrounding normal tissues. Its superior soft-tissue contrast and lack of ionizing radiation compared to CT makes it an attractive imaging modality, particularly for repeated imaging. However, there are still hurdles to be overcome, a major one being the lack of electron-density data for radiotherapy planning.

Anatomical structures within the prostate such as the apex and the seminal vesicles are more clearly visible on MRI than CT. This can lead to more accurate and precise outlining of the GTV using the MRI images than CT alone. T2 and DCE MRI imaging techniques aid in diagnosing sites of potential relapse. Vascular structures such as the corpus cavernosum internal pudental artery (IPA) that are involved in erectile function can be visualized using MR angiography and conventional coronal MRI imaging methods. These may be potential sites for conformal avoidance in future radiotherapy treatment regimens.

Use of MRI for the purposes of radiotherapy treatment planning, monitoring of tumor response over the course of treatment and assessment of relapse following treatment has been investigated for over a decade. Use of MRI for the purposes of radiotherapy contouring is considered the imaging modality of choice, with significant improvement in contrast between the target volume and normal tissues. MRI has been the imaging modality of choice for radiation therapy delineation for a number of clinical trials involving the cervix cancer-treatment site.

The debate over what field strength is optimum for MRI simulation remains inconclusive. Dedicated MR scanners for RT planning are presently being installed at both 1.5 and 3.0 Tesla. The utilization of MRI will certainly have a bearing on this; the soft-tissue anatomical delineation benefits are adequately provided for at 1.5 Tesla. However, the increase in signal-to-noise, which doubles by going to 3.0 Tesla, is important in signal hungry applications. This may be particularly useful for the functional techniques and in following treatment response. Generally imaging in the body is made more difficult at higher field strength due to increases in several artefacts and dielectric effects. Some of the RF homogeneity issues of the latter are now solved with the vendors providing dual transmit technology. Over the proceeding years those centres that have elected to install 3.0 Tesla should be able to provide data to make the optimal choice clearer.

Use of MRI for radiotherapy treatment planning is commonly undertaken to supplement CT imaging; this is still the standard of care. Radiotherapy treatment planning with MRI alone presents two challenges: the determination of electron density as required for accurate radiotherapy dose calculations; and geometrical accuracy. MRIs do not inherently provide any information on electron density and, particularly towards edge of the bore, may show significant distortion. A number of approaches have been undertaken to address these issues, with a methodologies being developed for radiotherapy treatment planning using MRI alone.

With the introduction of MRI-linear accelerators and the potential for real-time adaptive radiotherapy, geometric accuracy and electron-density accuracy will require

further investigation as treatment margins are reduced and the impact of geometry and dose-calculation errors is increased. The (ViewRay™) MRI-Cobalt machine is likely to give us the first window into how successful MR will be as an online image guidance modality. Sagittal images can be acquired using a fast 4 frame per second planar treatment scan that is based on the TRUFI (true fast imaging with steady state precession) sequence (89) known to provide the best SNR at very high speed among the existing fast imaging sequences. TRUFI is a type of fast gradient echo sequence (90).

Currently there are two working MRI-Linac prototypes. These include a modified 6 MV Elekta accelerator merged with a modified 1.5 T Philips Achieva MRI system with the linac beam transverse to the magnetic field (4). The transverse field approach results in numerous dose perturbation effects including the electron return effect, lateral dose shifting, cavity under and overdosing (91-93), and potentially large entry and exit skin dose increases (94, 95). These effects are reduced at low magnetic fields and multiple beam angles reduce the impact of skin dose. The other prototype includes a 6 MV accelerator merged with a biplanar, low field MRI (3, 96), whereby the linac and magnets can both rotate, hence enabling the linac beam to be in line with the magnetic field. This potentially also involves enhanced skin dose (5) from focused contamination. However clever design of the magnet may reduce this effect (97).

Conclusions

MRI has a proven role in stereotactic targeting in the brain; the potential for enhanced application of MRI in radiotherapy treatment planning to other cancer treatment sites in the body represents an exciting area of further research that deserves exploration. In the future the increased availability of dedicated scanners combined with the lack of ionising radiation make treatment planning using MRI alone a realistic and desirable prospect.

Experience has already shown that MR-only planning is feasible in brain (98), prostate (99) and several other areas (100). Developments in imaging sequences and bone-tissue segmentation combined with the production of good-quality pseudo-DRRs for patient set-up are all being investigated to further enhance this work. The logical progression of this MRI-guided strategy is the clinical prototyping of hybrid MRI-linear accelerator systems that will provide the ultimate in adaptive radiotherapy.

We hope this description of various MRI techniques applied to clinical trials indicates a pathway forward for enhanced use of MRI in TPS, leading perhaps to improved therapeutic ratio for patients and improved patient management in general. The breadth and scope of MRI sequences and analysis techniques is such that they can be considered analogous to opening a box of chocolates. One is never quite sure what is in the box but usually one is surprised by the sweetness of the outcome.

References

1. Tubiana, M. Can we reduce the incidence of second primary malignancies occurring after radiotherapy? A critical review. *Radiother Oncol 91*, 4-15 (2009). DOI: 10.1016/j.radonc.2008.12.016
2. Desar, I., Van Herpen, C., Van Laarhoven, H., Barentsz, J., Oyen, W., Van Der Graaf, W. Beyond RECIST: molecular and functional imaging techniques for evaluation of response to targeted therapy. *Cancer treatment reviews 35*, 309-321 (2009). DOI: 10.1016/j.ctrv.2008.12.001
3. Fallone, B., Carlone, M., Murray, B., Rathee, S., Stanescu, T., Steciw, S., Wachowicz, K., Kirkby, C. TU-C-M100F-01: Development of a linac-MRI system for real-time ART. *Medical Physics 34*, 2547 (2007). DOI: 10.1118/1.2761342
4. Raaymakers, B., Lagendijk, J., Overweg, J., Kok, J., Raaijmakers, A., Kerkhof, E., van der Put, R., Meijsing, I., Crijns, S., Benedosso, F. Integrating a 1.5 T MRI scanner with a 6 MV accelerator: proof of concept. *Physics in Medicine and Biology 54*, N229 (2009). DOI: 10.1088/0031-9155/54/12/N01
5. Oborn, B., Metcalfe, P., Butson, M., Rosenfeld, A., Keall, P. Electron contamination modeling and skin dose in 6 MV longitudinal field MRIgRT: Impact of the MRI and MRI fringe field. *Medical Physics 39*, 874 (2012). DOI: 10.1118/1.3676181
6. Raaymakers, B., Raaijmakers, A., Lagendijk, J. Feasibility of MRI guided proton therapy: magnetic field dose effects. *Physics in Medicine and Biology 53*, 5615 (2008). DOI: 10.1088/0031-9155/53/20/003
7. Mazaheri, Y., Shukla-Dave, A., Muellner, A., Hricak, H. MRI of the prostate: Clinical relevance and emerging applications. *Journal of Magnetic Resonance Imaging 33*, 258-274 (2011). DOI: 10.1002/jmri.22420
8. Philpotts, L. E. Comprehensive breast imaging 2010. *Seminars in Roentgenology 46*, 7-17 (2011). DOI: 10.1053/j.ro.2010.06.005
9. Hounsfield, G. N. Computerized transverse axial scanning (tomography): Part 1. Description of system. *British Journal of Radiology 46*, 1016-1022 (1973). DOI: 10.1259/0007-1285-46-552-1016
10. Metcalfe, P. E., Kron, T., Hoban, P. The physics of radiotherapy X-rays and electrons. (2007).
11. Garcia-Alvarez, R., Liney, G. P., Beavis, A. W. Repeatability of functional MRI for conformal avoidance radiotherapy planning. J*ournal of Magnetic Resonance Imaging 23*, 108-114 (2006). DOI: 10.1002/jmri.20493
12. Kovacs, A., Hadjiev, J., Lakosi, F., Antal, G., Vandulek, C., Somogyine Ezer, E., Bogner, P., Horvath, A., Repa, I. Dynamic MR based analysis of tumor movement in upper and mid lobe localized lung cancer. *Pathology & Oncology Research 15*, 269-277 (2009). DOI: 10.1007/s12253-008-9101-5

13. Ogawa, S., Lee, T. M., Nayak, A. S., Glynn, P. Oxygenation-sensitive contrast in magnetic resonance image of rodent brain at high magnetic fields. *Magnetic Resonance in Medicine 14*, 68-78 (1990). DOI: 10.1002/mrm.1910140108

14. Tofts, P. S., Brix, G., Buckley, D. L., Evelhoch, J. L., Henderson, E., Knopp, M. V., Larsson, H. B. W., Lee, T. Y., Mayr, N. A., Parker, G. J. M. Estimating kinetic parameters from dynamic contrast-enhanced T1-weighted MRI of a diffusable tracer: standardized quantities and symbols. *Journal of Magnetic Resonance Imaging 10*, 223-232 (1999). DOI: 10.1002/(SICI)1522-2586(199909)10:3<223::AID-JMRI2>3.0.CO;2-S

15. Vandecaveye, V., De Keyzer, F., Nuyts, S., Deraedt, K., Dirix, P., Hamaekers, P., Vander Poorten, V., Delaere, P., Hermans, R. Detection of head and neck squamous cell carcinoma with diffusion weighted MRI after (chemo) radiotherapy: correlation between radiologic and histopathologic findings. *International Journal of Radiation Oncology* Biology* Physics 67*, 960-971 (2007). DOI: 10.1016/j.ijrobp.2006.09.020

16. Srinivasan, A., Dvorak, R., Perni, K., Rohrer, S., Mukherji, S. Differentiation of benign and malignant pathology in the head and neck using 3T apparent diffusion coefficient values: early experience. *American Journal of Neuroradiology 29*, 40-44 (2008). DOI: 10.3174/ajnr.A0743

17. Bourne, R., Kurniawan, N., Cowin, G., Sved, P., Watson, G. 16 T Diffusion microimaging of fixed prostate tissue: preliminary findings. *Magnetic Resonance in Medicine 66*, 244-247 (2011). DOI: 10.1002/mrm.22778

18. Ling, C. C., Humm, J., Larson, S., Amols, H., Fuks, Z., Leibel, S., Koutcher, J. A. Towards multidimensional radiotherapy (MD-CRT): biological imaging and biological conformality. *International Journal of Radiation Oncology* Biology* Physics 47*, 551-560 (2000). DOI: 10.1016/S0360-3016(00)00467-3

19. Kim, Y., Tomé, W. A. Risk-adaptive optimization: selective boosting of high-risk tumor subvolumes. *International Journal of Radiation Oncology* Biology* Physics 66*, 1528-1542 (2006). DOI: 10.1016/j.ijrobp.2006.08.032

20. Star-Lack, J., Spielman, D., Adalsteinsson, E., Kurhanewicz, J., Terris, D. J., Vigneron, D. B. In vivo lactate editing with simultaneous detection of choline, creatine, NAA, and lipid singlets at 1.5 T using PRESS excitation with applications to the study of brain and head and neck tumors. *Journal of Magnetic Resonance 133*, 243-254 (1998). DOI: 10.1006/jmre.1998.1458

21. Kwock, L., Smith, J. K., Castillo, M., Ewend, M. G., Collichio, F., Morris, D. E., Bouldin, T. W., Cush, S. Clinical role of proton magnetic resonance spectroscopy in oncology: brain, breast, and prostate cancer. *The Lancet Oncology 7*, 859-868 (2006). DOI: 10.1016/S1470-2045(06)70905-6

22. Frahm, J., Haase, A., Matthaei, D. Rapid NMR imaging of dynamic processes using the FLASII technique. *Magnetic Resonance in Medicine 3*, 321-327 (1986). DOI: 10.1002/mrm.1910030217

23. Fain, S., Schiebler, M. L., McCormack, D. G., Parraga, G. Imaging of lung function using hyperpolarized helium-3 magnetic resonance imaging: review of current and emerging translational methods and applications. *Journal of Magnetic Resonance Imaging 32*, 1398-1408 (2010). DOI: 10.1002/jmri.22375

24. Hodge, C., Tomé, W. A., Fain, S., Bentzen, S., Mehta, M. On the use of hyperpolarized helium MRI for conformal avoidance lung radiotherapy. *Medical Dosimetry 35*, 297-303 (2011). DOI: 10.1016/j.meddos.2009.09.004

25. Adams, R. W., Aguilar, J. A., Atkinson, K. D., Cowley, M. J., Elliott, P. I. P., Duckett, S. B., Green, G. G. R., Khazal, I. G., López-Serrano, J., Williamson, D. C. Reversible interactions with para-hydrogen enhance NMR sensitivity by polarization transfer. *Science 323*, 1708-1711 (2009). DOI: 10.1126/science.1168877

26. Nelson, S., Vigneron, D., Kurhanewicz, J., Chen, A., Bok, R., Hurd, R. DNP-hyperpolarized 13 C magnetic resonance metabolic imaging for cancer applications. *Applied Magnetic Resonance 34*, 533-544 (2008). DOI: 10.1007/s00723-008-0136-2

27. Nelson, S. J., Cha, S. Imaging glioblastoma multiforme. *The Cancer Journal 9*, 134 (2003). DOI: 10.1097/00130404-200303000-00009

28. Essig, M., Schlemmer, H. P., Tronnier, V., Hawighorst, H., Wirtz, R., Van Kaick, G. Fluid-attenuated inversion-recovery MR imaging of gliomatosis cerebri. *European Radiology 11*, 303-308 (2001). DOI: 10.1007/s003300000587

29. Tomé, W. A., Mehta, M. P., Meeks, S. L., Buatti, J. M. Fractionated stereotactic radiotherapy: present and future. *Technol. in Cancer Res and Treat 1*, 153-172 (2002).

30. Petereit, D., Mehta, M., Turski, P., Levin, A., Strother, C., Mistretta, C., Mackie, R., Gehring, M., Kubsad, S., Kinsella, T. Treatment of arteriovenous malformations with stereotactic radiosurgery employing both magnetic resonance angiography and standard angiography as a database. *International Journal of Radiation Oncology*, Biology*, Physics 25*, 309-313 (1993). DOI: 10.1016/0360-3016(93)90353-W

31. Richards, G. M., Bradley, K. A., Tomé, W. A., Bentzen, S. M., Resnick, D. K., Mehta, M. P. Linear accelerator radiosurgery for trigeminal neuralgia. *Neurosurgery 57*, 1193 (2005). DOI: 10.1227/01.NEU.0000186015.01179.70

32. Hamstra, D. A., Galbán, C. J., Meyer, C. R., Johnson, T. D., Sundgren, P. C., Tsien, C., Lawrence, T. S., Junck, L., Ross, D. J., Rehemtulla, A. Functional diffusion map as an early imaging biomarker for high-grade glioma: correlation with conventional radiologic response and overall survival. *Journal of Clinical Oncology 26*, 3387-3394 (2008). DOI: 10.1200/JCO.2007.15.2363

33. Mardor, Y., Pfeffer, R., Spiegelmann, R., Roth, Y., Maier, S. E., Nissim, O., Berger, R., Glicksman, A., Baram, J., Orenstein, A. Early detection of response to radiation therapy in patients with brain malignancies using conventional and high *b*-value diffusion-weighted magnetic resonance imaging. *Journal of Clinical Oncology 21*, 1094-1100 (2003). DOI: 10.1200/JCO.2003.05.069

34. Kovács, Á., Tóth, L., Glavák, C., Liposits, G., Hadjiev, J., Antal, G., Emri, M., Vandulek, C., Repa, I. Integrating functional MRI information into conventional 3D radiotherapy planning of CNS tumors. Is it worth it? *Journal of Neurooncology 105*, 629-637 (2011). DOI: 10.1007/s11060-011-0633-2

35. Goldman, M., Boxerman, J. L., Rogg, J. M., Norén, G. Utility of apparent diffusion coefficient in predicting the outcome of gamma knife-treated brain metastases prior to changes in tumor volume: a preliminary study. *Special Supplements 105*, 175-182 (2006).

36. Chang, J., Thakur, S., Perera, G., Kowalski, A., Huang, W., Karimi, S., Hunt, M., Koutcher, J., Fuks, Z., Amols, H. Image-fusion of MR spectroscopic images for treatment planning of gliomas. *Medical Physics 33*, 32 (2006). DOI: 10.1118/1.2128497

37. Payne, G., Leach, M. Applications of magnetic resonance spectroscopy in radiotherapy treatment planning. *British Journal of Radiology 79*, S16-S26 (2006). DOI: 10.1259/bjr/84072695

38. Braams, J. W., Pruim, J., Freling, N., Nikkels, P., Roodenburg, J., Boering, G., Vaalburg, W., Vermey, A. Detection of lymph node metastases of squamous-cell cancer of the head and neck with FDG-PET and MRI. *Journal of Nuclear Medicine: Official Publication, Society of Nuclear Medicine 36*, 211 (1995).

39. Nishioka, T., Shiga, T., Shirato, H., Tsukamoto, E., Tsuchiya, K., Kato, T., Ohmori, K., Yamazaki, A., Aoyama, H., Hashimoto, S. Image fusion between 18 FDG-PET and MRI/CT for radiotherapy planning of oropharyngeal and nasopharyngeal carcinomas. *International Journal of Radiation Oncology* Biology* Physics 53*, 1051-1057 (2002). DOI: 10.1016/S0360-3016(02)02854-7

40. Al-Hallaq, H. A., Mell, L. K., Bradley, J. A., Chen, L. F., Ali, A. N., Weichselbaum, R. R., Newstead, G. M., Chmura, S. J. Magnetic resonance imaging identifies multifocal and multicentric disease in breast cancer patients who are eligible for partial breast irradiation. *Cancer 113*, 2408-2414 (2008). DOI: 10.1002/cncr.23872

41. Berg, W. A., Gutierrez, L., NessAiver, M. S., Carter, W. B., Bhargavan, M., Lewis, R. S., Ioffe, O. B. Diagnostic accuracy of mammography, clinical examination, US, and MR imaging in preoperative assessment of breast cancer. *Radiology 233*, 830-849 (2004). DOI: 10.1148/radiol.2333031484

42. Bluemke, D. A., Gatsonis, C. A., Chen, M. H., DeAngelis, G. A., DeBruhl, N., Harms, S., Heywang-Köbrunner, S. H., Hylton, N., Kuhl, C. K., Lehman, C. Magnetic resonance imaging of the breast prior to biopsy. *JAMA: The Journal of the American Medical Association 292*, 2735-2742 (2004). DOI: 10.1001/jama.292.22.2735

43. Fischer, U., Kopka, L., Grabbe, E. Breast carcinoma: effect of preoperative contrast-enhanced MR imaging on the therapeutic approach1. *Radiology 213*, 881-888 (1999).

44. Hata, T., Takahashi, H., Watanabe, K., Takahashi, M., Taguchi, K., Itoh, T., Todo, S. Magnetic resonance imaging for preoperative evaluation of breast cancer: a comparative study with mammography and ultrasonography. *Journal of the American College of Surgeons 198*, 190-197 (2004). DOI: 10.1016/j.jamcollsurg.2003.10.008

45. Pengel, K., Loo, C., Teertstra, H., Muller, S., Wesseling, J., Peterse, J., Bartelink, H., Rutgers, E., Gilhuijs, K. G. A. The impact of preoperative MRI on breast-conserving surgery of invasive cancer: a comparative cohort study. *Breast Cancer Research and Treatment 116*, 161-169 (2009). DOI: 10.1007/s10549-008-0182-3

46. Tendulkar, R. D., Chellman-Jeffers, M., Rybicki, L. A., Rim, A., Kotwal, A., Macklis, R., Obi, B. B. Preoperative breast magnetic resonance imaging in early breast cancer. *Cancer 115*, 1621-1630 (2009). DOI: 10.1002/cncr.24172

47. Uematsu, T., Yuen, S., Kasami, M., Uchida, Y. Comparison of magnetic resonance imaging, multidetector row computed tomography, ultrasonography, and mammography for tumor extension of breast cancer. *Breast Cancer Research and Treatment 112*, 461-474 (2008). DOI: 10.1007/s10549-008-9890-y

48. Van Goethem, M., Schelfout, K., Dijckmans, L., Van Der Auwera, J. C., Weyler, J., Verslegers, I., Biltjes, I., De Schepper, A. MR mammography in the pre-operative staging of breast cancer in patients with dense breast tissue: comparison with mammography and ultrasound. *European Radiology 14*, 809-816 (2004). DOI: 10.1007/s00330-003-2146-7

49. Hurkmans, C. W., Borger, J. H., Pieters, B. R., Russell, N. S., Jansen, E. P. M., Mijnheer, B. J. Variability in target volume delineation on CT scans of the breast. *International Journal of Radiation Oncology* Biology* Physics 50*, 1366-1372 (2001). DOI: 10.1016/S0360-3016(01)01635-2

50. Giezen, M., Kouwenhoven, E., Scholten, A. N., Coerkamp, E. G., Heijenbrok, M., Jansen, W. P. A., Mast, M. E., Petoukhova, A. L., Struikmans, H. Magnetic resonance imaging–versus computed tomography–based target volume delineation of the glandular breast tissue (clinical target volume breast) in breast-conserving therapy: an exploratory study. *International Journal of Radiation Oncology*, Biology*, Physics 81*, 804-811 (2011). DOI: 10.1016/j.ijrobp.2010.07.004

51. Jones, H. A., Antonini, N., Hart, A. A. M., Peterse, J. L., Horiot, J. C., Collin, F., Poortmans, P. M., Oei, S. B., Collette, L., Struikmans, H. Impact of pathological characteristics on local relapse after breast-conserving therapy: a subgroup analysis of the EORTC boost versus no boost trial. *Journal of Clinical Oncology 27*, 4939-4947 (2009). DOI: 10.1200/JCO.2008.21.5764

52. Ahn, K. H., Hargreaves, B. A., Alley, M. T., Horst, K. C., Luxton, G., Daniel, B. L., Hristov, D. MRI guidance for accelerated partial breast irradiation in prone position: imaging protocol design and evaluation. *International Journal of Radiation Oncology* Biology* Physics 75*, 285-293 (2009). DOI: 10.1016/j.ijrobp.2009.03.063

53. Kirby, A. M., Yarnold, J. R., Evans, P. M., Morgan, V. A., Schmidt, M. A., Scurr, E. D., deSouza, N. M. Tumor bed delineation for partial breast and breast boost radiotherapy planned in the prone position: what does MRI add to X-ray CT localization of titanium clips placed in the excision cavity wall? *International Journal of Radiation Oncology* Biology* Physics 74*, 1276-1282 (2009). DOI: 10.1016/j.ijrobp.2009.02.028

54. Schmitz, A. C., van den Bosch, M. A. A. J., Loo, C. E., Mali, W. P. T. M., Bartelink, H., Gertenbach, M., Holland, R., Peterse, J. L., Rutgers, E. J. T., Gilhuijs, K. G. Precise correlation between MRI and histopathology-exploring treatment margins for MRI-guided localized breast cancer therapy. *Radiotherapy and Oncology 97*, 225-232 (2010). DOI: 10.1016/j.radonc.2010.07.025

55. Mack, M. G., Balzer, J. O., Straub, R., Eichler, K., Vogl, T. J. Superparamagnetic iron oxide–enhanced MR imaging of head and neck lymph nodes1. *Radiology 222*, 239-244 (2002). DOI: 10.1148/radiol.2221010225

56. Plathow, C., Klopp, M., Fink, C., Sandner, A., Hof, H., Puderbach, M., Herth, F., Schmähl, A., Kauczor, H. Quantitative analysis of lung and tumour mobility: comparison of two time-resolved MRI sequences. *British Journal of Radiology 78*, 836-840 (2005). DOI: 10.1259/bjr/29483804

57. Blackall, J., Ahmad, S., Miquel, M., McClelland, J., Landau, D., Hawkes, D. MRI-based measurements of respiratory motion variability and assessment of imaging strategies for radiotherapy planning. *Physics in Medicine and Biology 51*, 4147 (2006). DOI: 10.1088/0031-9155/51/17/003

58. Plathow, C., Fink, C., Ley, S., Puderbach, M., Eichinger, M., Zuna, I., Schmähl, A., Kauczor, H. U. Measurement of tumor diameter-dependent mobility of lung tumors by dynamic MRI. *Radiotherapy and Oncology 73*, 349-354 (2004). DOI: 10.1016/j.radonc.2004.07.017

59. Cai, J., Read, P. W., Larner, J. M., Jones, D. R., Benedict, S. H., Sheng, K. Reproducibility of interfraction lung motion probability distribution function using dynamic MRI: statistical analysis. *International Journal of Radiation Oncology* Biology* Physics 72*, 1228-1235 (2008). DOI: 10.1016/j.ijrobp.2008.07.028

60. Mori, T., Nomori, H., Ikeda, K., Kawanaka, K., Shiraishi, S., Katahira, K., Yamashita, Y. Diffusion-weighted magnetic resonance imaging for diagnosing malignant pulmonary nodules/masses: comparison with positron emission tomography. *Journal of Thoracic Oncology 3*, 358 (2008). DOI: 10.1097/JTO.0b013e318168d9ed

61. Pauls, S., Breining, T., Muche, R., Schmidt, S. A., Wunderlich, A., Krüger, S., Brambs, H. J., Feuerlein, S. The role of dynamic, contrast-enhanced MRI in differentiating lung tumor subtypes. *Clinical Imaging 35*, 259 (2011). DOI: 10.1016/j.clinimag.2010.07.002

62. Bates, E. L., Bragg, C. M., Wild, J. M., Hatton, M. Q. F., Ireland, R. H. Functional image-based radiotherapy planning for non-small cell lung cancer: A simulation study. *Radiotherapy and Oncology 93*, 32-36 (2009). DOI: 10.1016/j.radonc.2009.05.018

63. Ireland, R. H., Bragg, C. M., McJury, M., Woodhouse, N., Fichele, S., van Beek, E. J. R., Wild, J. M., Hatton, M. Q. Feasibility of image registration and intensity-modulated radiotherapy planning with hyperpolarized helium-3 magnetic resonance imaging for non-small-cell lung cancer. *International Journal of Radiation Oncology* Biology* Physics 68*, 273-281 (2007). DOI: 10.1016/j.ijrobp.2006.12.068

64. Yankelevitz, D. F., Henschke, C. I., Batata, M., Kim, Y. S., Chu, F. Lung cancer: evaluation with MR imaging during and after irradiation. *Journal of Thoracic Imaging 9*, 41 (1994).

65. Hunter, G. J., Hamberg, L. M., Choi, N., Jain, R. K., McCloud, T., Fischman, A. J. Dynamic T1-weighted magnetic resonance imaging and positron emission tomography in patients with lung cancer: correlating vascular physiology with glucose metabolism. *Clinical Cancer Research 4*, 949-955 (1998).

66. Ohno, Y., Nogami, M., Higashino, T., Takenaka, D., Matsumoto, S., Hatabu, H., Sugimura, K. Prognostic value of dynamic MR imaging for non small cell lung cancer patients after chemoradiotherapy. *Journal of Magnetic Resonance Imaging 21*, 775-783 (2005). DOI: 10.1002/jmri.20297

67. Mcjury, M., O'Neill, A., Lawson, M., Mcgrath, C., Grey, A., Page, W., O'Sullivan, J. Assessing the image quality of pelvic MR images acquired with a flat couch for radiotherapy treatment planning. *British Journal of Radiology 84*, 750-755 (2011). DOI: 10.1259/bjr/27295679

68. Rosewall, T., Kong, V., Vesprini, D., Catton, C., Chung, P., Ménard, C., Bayley, A. Prostate delineation using CT and MRI for radiotherapy patients with bilateral hip prostheses. *Radiotherapy and Oncology 90*, 325-330 (2009). DOI: 10.1016/j.radonc.2008.11.015

69. Khoo, V., Padhani, A., Tanner, S., Finnigan, D., Leach, M., Dearnaley, D. Comparison of MRI with CT for the radiotherapy planning of prostate cancer: a feasibility study. *British Journal of Radiology 72*, 590-597 (1999).

70. Haider, M. A., Chung, P., Sweet, J., Toi, A., Jhaveri, K., Ménard, C., Warde, P., Trachtenberg, J., Lockwood, G., Milosevic, M. Dynamic contrast-enhanced magnetic resonance imaging for localization of recurrent prostate cancer after external beam radiotherapy. *International Journal of Radiation Oncology* Biology* Physics 70*, 425-430 (2008). DOI: 10.1016/j.ijrobp.2007.06.029

71. McLaughlin, P. W., Narayana, V., Meirowitz, A., Troyer, S., Roberson, P. L., Gonda, R., Sandler, H., Marsh, L., Lawrence, T., Kessler, M. Vessel-sparing prostate radiotherapy: dose limitation to critical erectile vascular structures (internal pudendal artery and corpus cavernosum) defined by MRI. *International Journal of Radiation Oncology* Biology* Physics 61*, 20-31 (2005). DOI: 10.1016/j.ijrobp.2004.04.070

72. van der Heide, U. A., Korporaal, J. G., Groenendaal, G., Franken, S., van Vulpen, M. Functional MRI for tumor delineation in prostate radiation therapy. *Imaging 3*, 219-231 (2011). DOI: 10.2217/iim.11.10

73. Chopra, S., Menard, C., Bristow, R., Toi, A., Milosevic, M., Haider, M. in *RöFo-Fortschritte auf dem Gebiet der Röntgenstrahlen und der bildgebenden Verfahren.* A2_2. DOI: 10.1055/s-0028-1085911

74. Jiménez De La Peña, M., Martínez de Vega Fernández, V., Recio Rodríguez, M., Carrascoso Arranz, J., Herráiz Hidalgo, L., Alvarez Moreno, E. Current imaging modalities in the diagnosis of cervical cancer. *Gynecologic Oncology 110*, S49-S54 (2008). DOI: 10.1016/j.ygyno.2008.05.030

75. Mitchell, D. G., Snyder, B., Coakley, F., Reinhold, C., Thomas, G., Amendola, M., Schwartz, L. H., Woodward, P., Pannu, H., Hricak, H. Early invasive cervical cancer: tumor delineation by magnetic resonance imaging, computed tomography, and clinical examination, verified by pathologic results, in the ACRIN 6651/GOG 183 Intergroup Study. *Journal of Clinical Oncology 24*, 5687-5694 (2006). DOI: 10.1200/JCO.2006.07.4799

76. Rockall, A. G., Sohaib, S. A., Harisinghani, M. G., Babar, S. A., Singh, N., Jeyarajah, A. R., Oram, D. H., Jacobs, I. J., Shepherd, J. H., Reznek, R. H. Diagnostic performance of nanoparticle-enhanced magnetic resonance imaging in the diagnosis of lymph node metastases in patients with endometrial and cervical cancer. *Journal of Clinical Oncology 23*, 2813-2821 (2005). DOI: 10.1200/JCO.2005.07.166

77. Dimopoulos, J. C. A., Schard, G., Berger, D., Lang, S., Goldner, G., Helbich, T., Pötter, R. Systematic evaluation of MRI findings in different stages of treatment of cervical cancer: potential of MRI on delineation of target, pathoanatomic structures, and organs at risk. *International Journal of Radiation Oncology* Biology* Physics 64*, 1380-1388 (2006). DOI: 10.1016/j.ijrobp.2005.10.017

78. Ozsarlak, O., Tjalma, W., Schepens, E., Corthouts, B., Beeck, B., Van Marck, E., Parizel, P., De Schepper, A. The correlation of preoperative CT, MR imaging, and clinical staging (FIGO) with histopathology findings in primary cervical carcinoma. *Eur Radiol 13*, 2338-2345 (2003). DOI: 10.1007/s00330-003-1928-2

79. Lim, K., Small, W. Jr, Portelance, L., Creutzberg, C., Jürgenliemk-Schulz, I. M., Mundt, A., Mell, L. K., Mayr, N., Viswanathan, A., Jhingran, A., Erickson, B., De Los Santos, J., Gaffney, D., Yashar, C., Beriwal, S., Wolfson, A., Taylor, A., Bosch, W., El Naqa, I., Fyles, A. Consensus Guidelines for delineation of clinical target volume for intensity-modulated pelvic radiotherapy for the definitive treatment of cervix cancer. *International Journal of Radiation Oncology*Biology*Physics 79*, 348-355 (2011). DOI: 10.1016/j.ijrobp.2009.10.075

80. Wu, D. H., Mayr, N. A., Karatas, Y., Karatas, R., Adli, M., Edwards, S. M., Wolff, J. D., Movahed, A., Montebello, J., Yuh, W. T. C. Interobserver variation in cervical cancer tumor delineation for image-based radiotherapy planning among and within different specialties. *Journal of Applied Clinical Medical Physics 6* (2005). DOI: 10.1120/jacmp.v6i4.2117

81. van de Bunt, L., van der Heide, U. A., Ketelaars, M., de Kort, G. A. P., Jürgenliemk-Schulz, I. M. Conventional, conformal, and intensity-modulated radiation therapy treatment planning of external beam radiotherapy for cervical cancer: The impact of tumor regression. *International Journal of Radiation Oncology*Biology*Physics 64*, 189-196 (2006). DOI: 10.1016/j.ijrobp.2005.04.025

82. van de Bunt, L., Jürgenliemk-Schulz, I. M., de Kort, G. A. P., Roesink, J. M., Tersteeg, R. J. H. A., van der Heide, U. A. Motion and deformation of the target volumes during IMRT for cervical cancer: What margins do we need? *Radiotherapy and Oncology 88*, 233-240 (2008). DOI: 10.1016/j.radonc.2007.12.017

83. Kerkhof, E. M., van der Put, R. W., Raaymakers, B. W., van der Heide, U. A., Jürgenliemk-Schulz, I. M., Lagendijk, J. J. W. Intrafraction motion in patients with cervical cancer: The benefit of soft tissue registration using MRI. *Radiotherapy and Oncology 93*, 115-121 (2009). DOI: 10.1016/j.radonc.2009.07.010

84. Levy, A., Caramella, C., Chargari, C., Medjhoul, A., Rey, A., Zareski, E., Boulet, B., Bidault, F., Dromain, C., Balleyguier, C. Accuracy of diffusion-weighted echo-planar MR imaging and ADC mapping in the evaluation of residual cervical carcinoma after radiation therapy. *Gynecologic Oncology* (2011). DOI: 10.1016/j.ygyno.2011.06.009

85. Chan, P., Dinniwell, R., Haider, M. A., Cho, Y.-B., Jaffray, D., Lockwood, G., Levin, W., Manchul, L., Fyles, A., Milosevic, M. Inter- and Intrafractional tumor and organ movement in patients with cervical cancer undergoing radiotherapy: a cinematic-MRI point-of-interest study. *International Journal of Radiation Oncology* Biology* Physics 70*, 1507-1515 (2008). DOI: 10.1016/j.ijrobp.2007.08.055

86. Hatano, K., Sekiya, Y., Araki, H., Sakai, M., Togawa, T., Narita, Y., Akiyama, Y., Kimura, S., Ito, H. Evaluation of the therapeutic effect of radiotherapy on cervical cancer using magnetic resonance imaging. *International Journal of Radiation Oncology*Biology*Physics 45*, 639-644 (1999). DOI: 10.1016/s0360-3016(99)00228-x

87. McVeigh, P., Syed, A., Milosevic, M., Fyles, A., Haider, M. Diffusion-weighted MRI in cervical cancer. *European Radiology 18*, 1058-1064 (2008). DOI: 10.1007/s00330-007-0843-3

88. Haie-Meder, C., Pötter, R., Van Limbergen, E., Briot, E., De Brabandere, M., Dimopoulos, J., Dumas, I., Hellebust, T. P., Kirisits, C., Lang, S. Recommendations from gynaecological (GYN) GEC-ESTRO working group: concepts and terms in 3D image based 3D treatment planning in cervix cancer brachytherapy with emphasis on MRI assessment of GTV and CTV. *Radiotherapy and Oncology 74*, 235-245 (2005). DOI: 10.1016/j.radonc.2004.12.015

89. Scheffler, K., Lehnhardt, S. Principles and applications of balanced SSFP techniques. *European Radiology 13*, 2409-2418 (2003). DOI: 10.1007/s00330-003-1957-x

90. Haase, A., Frahm, J., Matthaei, D., Hanicke, W., Merboldt, K. D. FLASH imaging. Rapid NMR imaging using low flip-angle pulses. *Journal of Magnetic Resonance (1969) 67*, 258-266 (1986).

91. Raaijmakers, A., Raaymakers, B., Lagendijk, J. Experimental verification of magnetic field dose effects for the

MRI-accelerator. *Physics in Medicine and Biology 52*, 4283 (2007). DOI: 10.1088/0031-9155/52/14/017

92. Raaijmakers, A., Raaymakers, B., Lagendijk, J. Magnetic-field-induced dose effects in MR-guided radiotherapy systems: dependence on the magnetic field strength. *Physics in Medicine and Biology 53*, 909 (2008). DOI: 10.1088/0031-9155/53/4/006

93. Raaijmakers, A., Raaymakers, B., Van der Meer, S., Lagendijk, J. Integrating a MRI scanner with a 6 MV radiotherapy accelerator: impact of the surface orientation on the entrance and exit dose due to the transverse magnetic field. *Physics in Medicine and Biology 52*, 929 (2007). DOI: 10.1088/0031-9155/52/4/005

94. Oborn, B. M., Metcalfe, P., Butson, M., Rosenfeld, A. High resolution entry and exit Monte Carlo dose calculations from a linear accelerator 6 MV beam under the influence of transverse magnetic fields. *Medical Physics 36*, 3549 (2009). DOI: 10.1118/1.3157203

95. Oborn, B. M., Metcalfe, P., Butson, M., Rosenfeld, A. Monte Carlo characterization of skin doses in 6 MV transverse field MRI-linac systems: effect of field size, surface orientation, magnetic field strength, and exit bolus. *Medical Physics 37*, 5208 (2010). DOI: 10.1118/1.3488980

96. Kirkby, C., Stanescu, T., Rathee, S., Carlone, M., Murray, B., Fallone, B. Patient dosimetry for hybrid MRI-radiotherapy systems. *Medical Physics 35*, 1019 (2008). DOI: 10.1118/1.2839104

97. Keyvanloo, A., Burke, B., Warkentin, B., Tadic, T., Rathee, S., Kirkby, C., Santos, D., Fallone, B. Skin dose in longitudinal and transverse linac-MRIs using Monte Carlo and realistic 3D MRI field models. *Medical Physics 39*, 6509 (2012). DOI: 10.1118/1.4754657

98. Beavis, A., Gibbs, P., Dealey, R., Whitton, V. Radiotherapy treatment planning of brain tumours using MRI alone. *British Journal of Radiology 71*, 544-548 (1998).

99. Lee, Y. K., Bollet, M., Charles-Edwards, G., Flower, M. A., Leach, M. O., McNair, H., Moore, E., Rowbottom, C., Webb, S. Radiotherapy treatment planning of prostate cancer using magnetic resonance imaging alone. *Radiotherapy and Oncology 66*, 203-216 (2003). DOI: 10.1016/S0167-8140(02)00440-1

100. Jonsson, J. H., Karlsson, M. G., Karlsson, M., Nyholm, T. Treatment planning using MRI data: an analysis of the dose calculation accuracy for different treatment regions. *Radiat Oncol 5*, 62 (2010). DOI: 10.1186/1748-717X-5-62